

ON THE NONLOCAL INTERACTION RANGE FOR STABILITY OF NANOBEMS WITH NONLINEAR DISTRIBUTION OF MATERIAL PROPERTIES

Piotr JANKOWSKI[✉]

*Faculty of Mechanical Engineering, Bialystok University of Technology, ul. Wiejska 45C, 15-351 Bialystok, Poland

p.jankowski@doktoranci.pb.edu.pl

received 17 January 2022, revised 10 February 2022, accepted 20 February 2022

Abstract: The present study analyses the range of nonlocal parameters' interaction on the buckling behaviour of nanobeam. The intelligent nonhomogeneous nanobeam is modelled as a symmetric functionally graded (FG) core with porosity cause nonlinear distribution of material parameters. The orthotropic face-sheets are made of piezoelectric materials. These kinds of structures are widely used in nanoelectromechanical systems (NEMS). The nanostructure model satisfies the assumptions of Reddy third-order beam theory and higher-order nonlocal elasticity and strain gradient theory. This approach allows to predict appropriate mechanical response of the nanobeam regardless of thin or thick structure, in addition to including nano-sized effects as hardening and softening. The analysis provided in the present study focuses on differences in results for nanobeam stability obtained based on classical and nonlocal theories. The study includes the effect of diverse size-dependent parameters, nanobeams' length-to-thickness ratio and distributions of porosity and material properties through the core thickness as well as external electro-mechanical loading. The results show a dependence of nonlocal interaction range on geometrical and material parameters of nanobeam. The investigation undertaken in the present study provides an interpretation for this phenomenon, and thus aids in increasing awareness of nanoscale structures' mechanical behaviour.

Key words: nanobeam, FGM, nonlocal strain gradient theory, buckling, piezoelectric effect

1. INTRODUCTION

Nanoelectromechanical systems (NEMS) generally refer to ultra-small structures that combine mechanical and electrical components in one device. These devices may find applications as force and displacement sensors [1], mass sensors [2], energy harvesters [3] electromechanical actuators [4]. Further, buckling behaviour plays a crucial role in the operation of these devices [5].

Small-scale effects should be considered in the prediction of the appropriate mechanical behaviour of micro- and nanostructures [6]. Therefore, nonlocal theories have modified classical continuum theories in three different ways. The strain gradient ones, which include the couple stress theory [7-9], the modified couple stress theory [10] and Mindlin's strain gradient theories [11,12], as well as the modified strain gradient theory [13], are based on assumption that the mechanical response of small-scaled structures depends on strains and gradients of strains. This approach is correlated with stiffness hardening effects. On the other hand, stress-gradient-based theories were established on the assumption that ultra-small-scale structures' mechanical behaviour depends on stress and gradients of stress. This approach is related to constitutive equations expressed by integral form [14-17] and differential form [18], as well as integrodifferential form [19]. These procedures capture mainly stiffness softening phenomena but hardening effect can be found in special cases. Nevertheless, in nanostructures' experiments, hardening-softening stiffness phenomena are observed [20,21]. A subsequent method that combines advantages of strain gradient and nonlocal elasticity theories was proposed as a higher-order non-

local elasticity and strain gradient theory [22,23]. The aforementioned theory, known as the nonlocal strain gradient theory, employs nonlocal coefficient and length scale parameters to include both stiffness softening and hardening effects. Another advantage is that by reducing the related parameters, it becomes possible to easily obtain the required results through the strain gradient approach, nonlocal elasticity, or even classical continuum theory [6].

Increasing range of small-scaled devices' applications in various technology fields resulted in researchers' interest in modelling diverse structures' size-dependent mechanical response using various variational and nonlocal approaches. Among these, one can include ultra-small structures' dynamic response including torsional and longitudinal vibrations [24-26], vibrations under buckyballs [27], and considering thermal [28], magnetic [29], magneto-electro-elastic [30], and flexoelectric [31] effects. Deflection analysis of micro/nano structures involves influence of diverse load distributions [32-35], magnetic [36] and magneto-electric [37] phenomena, hydrothermal environment [38,39], or novel nonlocal approaches [40] and nonlocal boundary conditions [41].

In order to maintain a subject matter similar to the study, the literature review is focused on a buckling response of nano-sized beam structures. Reddy [42] compared the influence of nonlocal parameter on bending, buckling and vibration for various beam theories based on analytical solution for simply supported nanostructures. Aydogdu [43] compared exponential beam theory with other models in analysing bending, buckling and vibration of Eringen's nanobeam. Roque et al. [44] proposed a meshless method to study bending, buckling and vibrations of nanobeam based on Eringen's nonlocal elasticity, Timoshenko beam model and two different collocation techniques. Thai [45] and Thai and

Vo [46] presented an analytical solution for free vibration, bending and buckling of nanobeam based on newly proposed refined higher-order shear deformation and sinusoidal shear deformation beam models using assumptions of Eringen's nonlocal elasticity. Ghannadpour et al. [47] studied the bending, buckling and vibration characteristics of nonlocal Euler-Bernoulli beam model for diverse boundary conditions (BCs) utilising the Ritz technique to solve defined problems. Şimşek and Yurtcu [48] compared bending and buckling of Euler-Bernoulli and Timoshenko functionally graded (FG) nanobeams based on Eringen's nonlocal theory for simply supported boundary conditions (BCs) using Navier solution procedure. Rahmani and Jandaghian [49] employed Eringen's nonlocal theory and Reddy displacement field to investigate buckling of FG nanobeam for various BCs using Rayleigh–Ritz method. Chaht [50] investigated the effect of Eringen's nonlocal parameter on bending and buckling of simply supported FG nanobeam using sinusoidal shear deformation theory with thickness stretching. Yu et al. [51] analysed the effect of heat conduction on buckling response of nanobeam for diverse BCs based on Eringen's nonlocal theory and Euler-Bernoulli beam model. Nejad et al. [52] conducted a study on buckling behaviour of Euler-Bernoulli two-dimensional FG nanobeam for diverse BCs based on nonlocal elasticity and generalised differential quadrature method (GDQM). Li et al. [53] employed nonlocal strain gradient theory and Euler-Bernoulli beam model to study bending, buckling and vibration of axially FG nanobeam by using GDQM approach. Tuna and Kirca [54] proposed finite element model formulation to investigate bending, buckling and free vibration problem of Eringen's nanobeam with various BCs. Mirjavadi et al. [55] analysed buckling and vibration of FG Euler-Bernoulli nanobeam including von-Karman strains and various BCs, using nonlocal elasticity and GDQM. Khaniki et al. [56] studied buckling in nonuniform Euler-Bernoulli nanobeam in the context of nonlocal strain gradient theory and numerical meshless approach. Alibeigi et al. [57,58] studied the nonlinear bending and buckling behaviours of piezoelectric and piezomagnetic nanobeam in thermal, electrical and mechanical environments in the context of modified couple stress theory and Galerkin approach. Xiao et al. [59] discussed nonlinear thermal buckling of FG porous nanobeam, including magneto-electro-elastic coupling effects using Eringen's nonlocal theory and perturbation solution method. Hashemian et al. [60] utilised Navier solution technique and nonlocal strain gradient theory to compare the influence of small-scale effect on bending and buckling response on nanobeams modelled by various beam theories. Jankowski et al. [61] conducted a study on buckling and vibration of FG porous nanobeam based on nonlocal strain gradient theory together with Reddy third-order and Timoshenko beam theories. Civalek et al. [62,63] proposed finite element formulation to analyse buckling of nanobeam-based structures for different BCs using Euler-Bernoulli assumptions and Eringen's nonlocal elasticity as well as modified couple stress theory.

1.1. Novelty of the paper

Given the constant development of nanoscience and nanotechnology, modelling of ultra-small structures deserves to be recognised as an important issue that scientists in the current era need to deal with. Nevertheless, based on the provided literature survey, it can be gauged that the range of nonlocal interaction for nanostructures has not been investigated yet. There is still a lack

of adequate knowledge of nonlocal and length scale parameters' impact on nanostructures' mechanical behaviour, considering the effect of its geometrical as well as material properties or external loads. The present study supplements the research gap by providing a size-dependent buckling analysis of three-layered functionally graded material (FGM) piezoelectric nanobeam. Utilized Reddy third-order shear deformation theory may to an analysis of thick as well as thin structures. Additionally, the beam model does not require a shear correction factor, which should be determined separately for different material parameters' variations, geometric ratios and loadings. Therefore, the theory employed in the present study ensures high accuracy and makes it possible to omit the drawbacks of other theories. In comparison to previous studies [61,64] the present investigation ensures another perspective to size-dependent buckling response of nanobeam. The paper is focused on a range of nonlocal effects on nanostructure mechanical response in view of material and geometrical properties as well as electromechanical loads. The current investigation presents differences, regarding classical continuum theory, of mechanical response of nanostructures taking into account diverse relations of small-scale coefficients together with length to thickness ratios, influence of mechanical forces and electric field, properties of FG material gradation along with distribution and volume of porosity. The present study will widen the understanding of the size-dependent responses of nanostructures and increase awareness about the necessity to use, or alternatively the unfavourable consequences of omitting, nonlocal theories in the modelling of nanoscale smart structures, which is a key value in optimisation and control of NEMS devices.

2. CONSTITUTIVE RELATIONS

One of the favoured theories including size-dependent phenomena is nonlocal elasticity proposed by [15,16,18,65], which postulates that stress at a point in continuum depends on the strain at that point as well at points in the whole domain. On the other hand, theories employing strain-gradient-based assumptions [7-9,11,12] state that materials should not be treated as a collection of points, but rather as atoms with higher-order deformation mechanism at micro- and nanoscales. Askes and Aifantis [22] and Lim et al. [23] found it necessary to bring together two entirely different physical phenomena into a single theory to describe a more real structural response at the nanoscale. The higher-order nonlocal elasticity and strain gradient theory combines nonlocal assumptions of strain gradient and stress gradient. The theory captures both nonlocal phenomena and consequently enables a more effective prediction of the size-dependent mechanical response. Based on the refined theory assumptions, the total stress tensor of the nonlocal strain gradient theory is defined as

$$\boldsymbol{\sigma} = \bar{\boldsymbol{\sigma}} - \nabla \bar{\boldsymbol{\sigma}}^{(1)} \quad (1)$$

where $\nabla = \mathbf{e}_i \frac{d}{dx_i}$ is the vector differential operator, in which \mathbf{e}_i is the unit vector and x_i is considered the direction of a nonlocal effect in a structure. Then, $\bar{\boldsymbol{\sigma}}$ and $\bar{\boldsymbol{\sigma}}^{(1)}$ are classical and higher-order stress tensor, respectively. The three-dimensional components are

$$\bar{\boldsymbol{\sigma}} = \int_V \alpha_0(\mathbf{x}', \mathbf{x}, e_0 a) \mathbf{C} : \boldsymbol{\varepsilon}' dV' \quad (2a)$$

$$\bar{\sigma}^{(1)} = \ell^2 \int_V \alpha_1(\mathbf{x}', \mathbf{x}, e_1 a) \mathbf{C} : \nabla \varepsilon' dV' \quad (2b)$$

where $\alpha_0(\mathbf{x}', \mathbf{x}, e_0 a)$ is the principal attenuation kernel function related to the nonlocality in terms of Euclidean distance between the point \mathbf{x} and points \mathbf{x}' in the domain V , and $\alpha_1(\mathbf{x}', \mathbf{x}, e_1 a)$ is the additional attenuation kernel function introduced to describe the nonlocal effect of first-order strain gradient field. Subsequently, ℓ is the material length scale coefficient that describes the higher-order strain gradient field, a is internal characteristic length (e.g., interatomic distance) and e_0 and e_1 are the nonlocal material constants. ε , ε' and \mathbf{C} represent the strain tensor, the strain gradient tensor and the fourth-order elastic modulus tensor, respectively. Applying the linear differential operators in form

$$\mathbf{L}_i = 1 - (e_i a)^2 \nabla^2, \quad i = 0, 1 \quad (3)$$

on both sides of Eq. (1) leads to a general differential form of the constitutive equations based on the higher-order nonlocal strain gradient theory, including three length scale parameters: two of them for nonlocal stress and the third for strain gradients

$$[1 - (e_1 a)^2 \nabla^2][1 - (e_0 a)^2 \nabla^2] \sigma = [1 - (e_1 a)^2 \nabla^2] \mathbf{C} : \varepsilon - \ell^2 [1 - (e_0 a)^2 \nabla^2] \nabla \mathbf{C} : \nabla \varepsilon \quad (4)$$

Assuming that $e_1 = e_0 = e$, one can obtain a simplified model in the form

$$[1 - (ea)^2 \nabla^2] \sigma = [1 - \nabla^2 \ell^2] \mathbf{C} : \varepsilon \quad (5)$$

The presented model may be easily reduced to stress-based Eringen's nonlocal elasticity taking $\ell = 0$:

$$[1 - (ea)^2 \nabla^2] \sigma = \mathbf{C} : \varepsilon \quad (6)$$

Alternatively, supposing $ea = 0$ indicates the form of Mindlin's strain gradient theory

$$\sigma = [1 - \nabla^2 \ell^2] \mathbf{C} : \varepsilon \quad (7)$$

Considering the above, constitutive relations for present investigation are

$$(1 - \mathfrak{B} \nabla^2) \sigma_{xx} = (1 - \ell^2 \nabla^2) C_{xx} \varepsilon_{xx} \quad (8a)$$

$$(1 - \mathfrak{B} \nabla^2) \sigma_{xz} = (1 - \ell^2 \nabla^2) 2C_{xz} \varepsilon_{xz} \quad (8b)$$

where $\mathfrak{B} = (ea)^2$ and differential operator takes the unidirectional form $\nabla^2 = \frac{\partial^2}{\partial x^2}$.

3. DISPLACEMENT FIELD AND MATERIAL PROPERTIES

Consider a symmetric FG nanobeam layered with piezoelectric face-sheets characterised by length L , width b and total thickness $H = h + 2h_p$ that consists of a core made of porous FGM with thickness h , and two piezoelectric layers thicknesses h_p . An ideal mechanical contact is assumed between the FGM core and other layers, which is more justified for structures at nanoscales, owing to possible strong bonds, e.g., chemical bonds. The nanobeam is under electric field induced by external initial electric voltage ϕ_0 and under mechanical load presented as axial in-plane forces \bar{N}_{xx} . The nanostructure coordinate system and its cross-section are illustrated in Fig. 1.

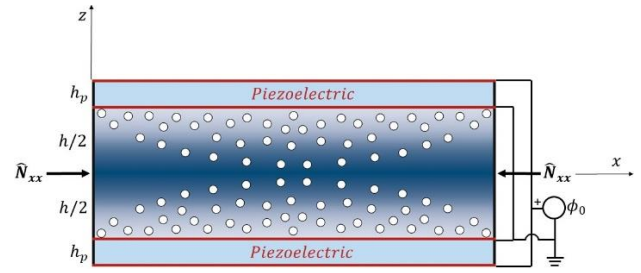


Fig. 1. Model of three-layered porous FGM nanobeam subjected to external mechanical loads and electric field

3.1. Displacement field

Based on assumptions of Reddy third-order shear deformation beam theory [66], the displacement field takes the form

$$u_x(x, z, t) = u_0(x, t) + z\varphi_x(x, t) - c_1 z^3 \left(\varphi_x(x, t) + \frac{\partial w_0(x, t)}{\partial x} \right) \quad (9a)$$

$$u_z(x, t) = w_0(x, t) \quad (9b)$$

where u_x and u_z are the total displacement vector components, and particular elements u_0 , w_0 are displacements in axial and transverse directions of a material point in the midplane in the undeformed configuration at any time t . φ_x represents the rotation of the point on the centroidal axis x of the beam, and $c_1 = 4/(3H^2)$.

Assuming linear and infinitesimal Green–Lagrange strain tensor ε , strain–displacement relations are presented as

$$\varepsilon_{xx} = \varepsilon_{xx}^{(0)} + z\varepsilon_{xx}^{(1)} + z^3\varepsilon_{xx}^{(3)} \quad (10a)$$

$$2\varepsilon_{xz} = \gamma_{xz}^{(0)} + z^2\gamma_{xz}^{(2)} \quad (10b)$$

with particular components

$$\{\varepsilon_{xx}^{(0)}, \varepsilon_{xx}^{(1)}, \varepsilon_{xx}^{(3)}\} = \left\{ \frac{\partial u_0}{\partial x}, \frac{\partial \varphi_x}{\partial x}, -c_1 \left(\frac{\partial \varphi_x}{\partial x} + \frac{\partial^2 w_0}{\partial x^2} \right) \right\} \quad (11a)$$

$$\{\gamma_{xz}^{(0)}, \gamma_{xz}^{(2)}\} = \left\{ \varphi_x + \frac{\partial w_0}{\partial x}, -c_2 \left(\varphi_x + \frac{\partial w_0}{\partial x} \right) \right\} \quad (11b)$$

where $c_2 = 3c_1$.

3.2. Material properties for FGM core

The presented nanobeam consists of orthotropic piezoelectric face-sheets and FG porous core with a presumption of perfect mechanical connection between each layer. The stiffness coefficients of the porous FGM nanobeam core are described as:

$$C_{xx} = E(z, Y) \quad (12a)$$

$$C_{xz} = \frac{E(z, Y)}{2(1+\nu)} \quad (12b)$$

where ν is Poisson's ratio that is assumed to be constant due to low volatility of the coefficient, and consequently, with minor influence on mechanical response. $E(z, Y)$ is Young's modulus that varies through the nanobeam core thickness h for different porosity distribution Y in the volume. Material properties of symmetric (with respect to the midplane $z = 0$) FG structure with porosity are described based on modified Voigt's rule of mixtures as follows [64]:

$$E^{(n)}(z) = [(E_c - E_m)V^{(n)}(z, g) + E_m][1 - Y(z, \vartheta)] \quad (13)$$

where E_c and E_m refer to Young's modulus of ceramic and metal in the upper and lower surfaces that consist of the mixture inside the structure. The volume fraction function $V^{(n)}$ of the n th layer is defined as:

$$V^{(1)} = \left(\frac{z+\frac{h}{2}}{\frac{h}{2}}\right)^g \quad \wedge \quad z \in \left\langle -\frac{h}{2}, 0 \right\rangle \quad (14a)$$

$$V^{(2)} = \left(\frac{\frac{z-\frac{h}{2}}{-\frac{h}{2}}}{\frac{h}{2}}\right)^g \quad \wedge \quad z \in \left\langle 0, \frac{h}{2} \right\rangle \quad (14b)$$

The power-law index g controls the share of constituents in the resultant structure. Diverse porosity distributions are modelled using function $Y(z, \vartheta)$. In the present study, three diverse porosity distributions [64] are examined, as under:

$$\text{Type 1: } Y(z, \vartheta) = \vartheta \cos\left(\frac{\pi z}{h}\right) \quad \wedge \quad z \in \left\langle -\frac{h}{2}, \frac{h}{2} \right\rangle \quad (15a)$$

$$\text{Type 2: } Y(z, \vartheta) = \begin{cases} \vartheta \cos\left[\pi\left(\frac{2z}{h} + \frac{1}{2}\right)\right] & \wedge \quad z \in \left\langle -\frac{h}{2}, 0 \right\rangle \\ \vartheta \cos\left[\pi\left(\frac{2z}{h} - \frac{1}{2}\right)\right] & \wedge \quad z \in \left\langle 0, \frac{h}{2} \right\rangle \end{cases} \quad (15b)$$

$$\text{Type 3: } Y(z, \vartheta) = \begin{cases} \vartheta \cos\left[\pi\left(\frac{z}{h} + \frac{1}{2}\right)\right] & \wedge \quad z \in \left\langle -\frac{h}{2}, 0 \right\rangle \\ \vartheta \cos\left[\pi\left(\frac{z}{h} - \frac{1}{2}\right)\right] & \wedge \quad z \in \left\langle 0, \frac{h}{2} \right\rangle \end{cases} \quad (15c)$$

where ϑ is porosity coefficient that determines maximum volume of voids. Material properties, as well as distributions of porosity through the nanobeam core thickness, are presented in Fig. 2.

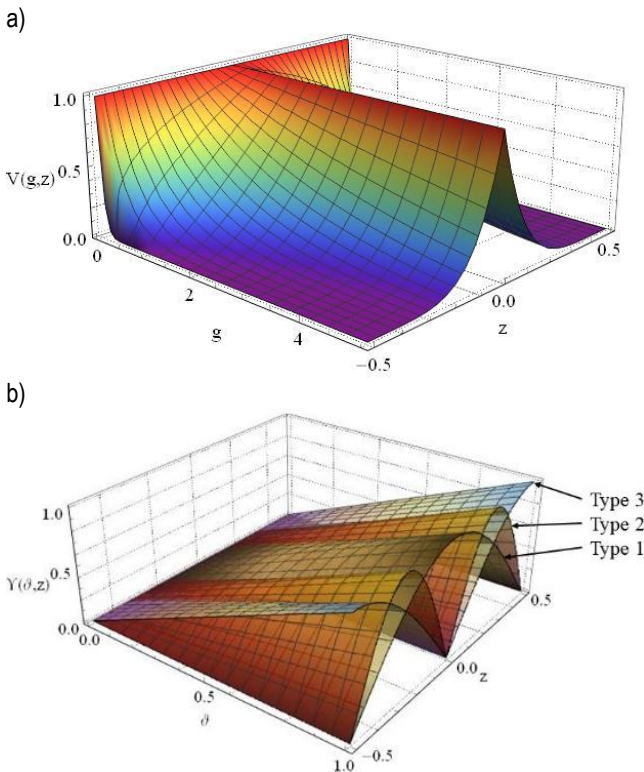


Fig. 2. Properties of nanobeams FGM core: (a) volume fraction function; (b) distribution of porosity

3.3. Piezoelectric characteristics

The electric field is described based on a combination of the half-cosine and linear variations of the electric potential Φ [67]:

$$\Phi(x, z, t) = -\cos\left(\frac{\pi z_p}{h_p}\right)\Phi(x, t) + \frac{2z_p}{h_p}\phi_0 \quad (16)$$

where $\Phi(x, t)$ refers to plane time-dependent distribution of electric potential and ϕ_0 is an initial external voltage. A new variable z_p is measured from the geometrical centre of the piezoelectric layers, and thus $z_1 = z - h/2 - h_p/2$ and $z_2 = z + h/2 + h_p/2$ are defined for the top and bottom layers, respectively. Based on the electric potential function, the components of electric field E_i are obtained, using a derivative with respect to the appropriate coordinate, as the following:

$$E_x = -\frac{\partial \Phi}{\partial x} = \cos\left(\frac{\pi z_p}{h_p}\right)\frac{\partial \Phi}{\partial x} \quad (17a)$$

$$E_z = -\frac{\partial \Phi}{\partial z} = -\frac{\pi}{h_p}\sin\left(\frac{\pi z_p}{h_p}\right)\Phi - \frac{2}{h_p}\phi_0 \quad (17b)$$

According to the nonlocal strain gradient theory, as well as obtained material properties together with electric field contribution, the final form of constitutive relations [64] is presented as follows:

$$(1 - \mathfrak{B}\nabla^2)\sigma_{xx}^p = (1 - \ell^2\nabla^2)(D_{xx}\varepsilon_{xx} - e_x E_z) \quad (18a)$$

$$(1 - \mathfrak{B}\nabla^2)\sigma_{xz}^p = (1 - \ell^2\nabla^2)(2D_{xz}\varepsilon_{xz} - e_z E_x) \quad (18b)$$

$$(1 - \mathfrak{B}\nabla^2)D_x^p = (1 - \ell^2\nabla^2)(2e_z\varepsilon_{xz} + \varepsilon_x E_x) \quad (18c)$$

$$(1 - \mathfrak{B}\nabla^2)D_z^p = (1 - \ell^2\nabla^2)(e_x\varepsilon_{xx} + \varepsilon_z E_z) \quad (18d)$$

$$(1 - \mathfrak{B}\nabla^2)\sigma_{xx}^c = (1 - \ell^2\nabla^2)C_{xx}\varepsilon_{xx} \quad (19a)$$

$$(1 - \mathfrak{B}\nabla^2)\sigma_{xz}^c = (1 - \ell^2\nabla^2)2C_{xz}\varepsilon_{xz} \quad (19b)$$

where superscripts p and c refer to the piezoelectric layers and FGM core, respectively, and D_i^p stands for electric displacement components. Additionally, D_{ij} represent the piezoelectric layers' stiffness coefficient and e_i and ε_i are, respectively, piezoelectric and dielectric permittivity constants.

4. EQUATIONS OF MOTION AND SOLUTION

4.1. Equations of motion

The equations of motion of the studied nanobeam are derived based on the modified Hamilton's variational principle, in the form

$$\int_0^T (\delta\mathcal{U} - \delta\mathcal{E} + \delta\mathcal{V})dt = 0 \quad (20)$$

where $\delta\mathcal{U}$, $\delta\mathcal{E}$ and $\delta\mathcal{V}$ stands for variations of virtual strain energy, virtual contribution of electric field and virtual work done by external forces, respectively. The procedure that leads to deriving equations of motion expressed by generalised displacements, including nonlocal interaction, is comprehensively described in a previous paper [64]. In the current study, we used previously derived equations of motion, which can be expressed as the following:

$$A_{xx}^{(0)} \frac{\partial^2 u_0}{\partial x^2} + A_{xx}^{(1)} \frac{\partial^2 \varphi_x}{\partial x^2} - c_1 A_{xx}^{(3)} \left(\frac{\partial^2 \varphi_x}{\partial x^2} + \frac{\partial^3 w_0}{\partial x^3} \right) + B_x^{(0)} \frac{\partial \Phi}{\partial x} - \rho^2 \left[A_{xx}^{(0)} \frac{\partial^4 u_0}{\partial x^4} + A_{xx}^{(1)} \frac{\partial^4 \varphi_x}{\partial x^4} - c_1 A_{xx}^{(3)} \left(\frac{\partial^4 \varphi_x}{\partial x^4} + \frac{\partial^5 w_0}{\partial x^5} \right) + B_x^{(0)} \frac{\partial^3 \Phi}{\partial x^3} \right] = 0 \quad (21a)$$

$$-A_{xx}^{(0)} \left(\varphi_x + \frac{\partial w_0}{\partial x} \right) + 2c_2 A_{xz}^{(2)} \left(\varphi_x + \frac{\partial w_0}{\partial x} \right) - c_2^2 A_{xz}^{(4)} \left(\varphi_x + \frac{\partial w_0}{\partial x} \right) + A_{xx}^{(1)} \frac{\partial^2 u_0}{\partial x^2} - c_1 A_{xx}^{(3)} \frac{\partial^2 u_0}{\partial x^2} + A_{xx}^{(2)} \frac{\partial^2 \varphi_x}{\partial x^2} - c_1 A_{xx}^{(4)} \frac{\partial^2 \varphi_x}{\partial x^2} - c_1 A_{xx}^{(4)} \left(\frac{\partial^2 \varphi_x}{\partial x^2} + \frac{\partial^3 w_0}{\partial x^3} \right) + c_1^2 A_{xx}^{(6)} \left(\frac{\partial^2 \varphi_x}{\partial x^2} + \frac{\partial^3 w_0}{\partial x^3} \right) + B_z^{(0)} \frac{\partial \Phi}{\partial x} + B_x^{(1)} \frac{\partial \Phi}{\partial x} - c_1 B_x^{(3)} \frac{\partial \Phi}{\partial x} - c_2 B_z^{(2)} \frac{\partial \Phi}{\partial x} - \rho^2 \left[-A_{xz}^{(0)} \left(\frac{\partial^2 \varphi_x}{\partial x^2} + \frac{\partial^3 w_0}{\partial x^3} \right) + 2c_2 A_{xz}^{(2)} \left(\frac{\partial^2 \varphi_x}{\partial x^2} + \frac{\partial^3 w_0}{\partial x^3} \right) - c_2^2 A_{xz}^{(4)} \left(\frac{\partial^2 \varphi_x}{\partial x^2} + \frac{\partial^3 w_0}{\partial x^3} \right) + A_{xx}^{(1)} \frac{\partial^4 u_0}{\partial x^4} - c_1 A_{xx}^{(3)} \frac{\partial^4 u_0}{\partial x^4} + A_{xx}^{(2)} \frac{\partial^4 \varphi_x}{\partial x^4} - c_1 A_{xx}^{(4)} \frac{\partial^4 \varphi_x}{\partial x^4} - c_1 A_{xx}^{(4)} \left(\frac{\partial^4 \varphi_x}{\partial x^4} + \frac{\partial^5 w_0}{\partial x^5} \right) + c_1^2 A_{xx}^{(6)} \left(\frac{\partial^4 \varphi_x}{\partial x^4} + \frac{\partial^5 w_0}{\partial x^5} \right) + B_x^{(1)} \frac{\partial^3 \Phi}{\partial x^3} + B_z^{(0)} \frac{\partial^3 \Phi}{\partial x^3} - c_1 B_x^{(3)} \frac{\partial^3 \Phi}{\partial x^3} - c_2 B_z^{(2)} \frac{\partial^3 \Phi}{\partial x^3} \right] = 0 \quad (21b)$$

$$c_1 A_{xx}^{(3)} \frac{\partial^3 u_0}{\partial x^3} + A_{xz}^{(0)} \left(\frac{\partial \varphi_x}{\partial x} + \frac{\partial^2 w_0}{\partial x^2} \right) - 2c_2 A_{xz}^{(2)} \left(\frac{\partial \varphi_x}{\partial x} + \frac{\partial^2 w_0}{\partial x^2} \right) + c_2^2 A_{xz}^{(4)} \left(\frac{\partial \varphi_x}{\partial x} + \frac{\partial^2 w_0}{\partial x^2} \right) + c_1 A_{xx}^{(4)} \frac{\partial^3 \varphi_x}{\partial x^3} - c_1^2 A_{xx}^{(6)} \left(\frac{\partial^3 \varphi_x}{\partial x^3} + \frac{\partial^4 w_0}{\partial x^4} \right) - B_z^{(0)} \frac{\partial^2 \Phi}{\partial x^2} + c_2 B_z^{(2)} \frac{\partial^2 \Phi}{\partial x^2} + c_1 B_x^{(3)} \frac{\partial^2 \Phi}{\partial x^2} - \rho^2 \left[c_1 A_{xx}^{(3)} \frac{\partial^5 u_0}{\partial x^5} + A_{xz}^{(0)} \left(\frac{\partial^3 \varphi_x}{\partial x^3} + \frac{\partial^4 w_0}{\partial x^4} \right) - 2c_2 A_{xz}^{(2)} \left(\frac{\partial^3 \varphi_x}{\partial x^3} + \frac{\partial^4 w_0}{\partial x^4} \right) + c_2^2 A_{xz}^{(4)} \left(\frac{\partial^3 \varphi_x}{\partial x^3} + \frac{\partial^4 w_0}{\partial x^4} \right) + c_1 A_{xx}^{(4)} \frac{\partial^5 \varphi_x}{\partial x^5} - c_1^2 A_{xx}^{(6)} \left(\frac{\partial^5 \varphi_x}{\partial x^5} + \frac{\partial^6 w_0}{\partial x^6} \right) - B_z^{(0)} \frac{\partial^4 \Phi}{\partial x^4} + c_1 B_x^{(3)} \frac{\partial^4 \Phi}{\partial x^4} + c_2 B_z^{(2)} \frac{\partial^4 \Phi}{\partial x^4} \right] = \hat{N}_\varepsilon \frac{\partial^2 w_0}{\partial x^2} + \hat{N}_{xx} \frac{\partial^2 w_0}{\partial x^2} - \mathfrak{B} \left[\hat{N}_\varepsilon \frac{\partial^4 w_0}{\partial x^4} + \hat{N}_{xx} \frac{\partial^4 w_0}{\partial x^4} \right] \quad (21c)$$

$$B_x^{(0)} \frac{\partial u_0}{\partial x} + B_x^{(1)} \frac{\partial \varphi_x}{\partial x} + B_z^{(0)} \left(\frac{\partial \varphi_x}{\partial x} + \frac{\partial^2 w_0}{\partial x^2} \right) - c_1 B_x^{(3)} \left(\frac{\partial \varphi_x}{\partial x} + \frac{\partial^2 w_0}{\partial x^2} \right) - c_2 B_z^{(2)} \left(\frac{\partial \varphi_x}{\partial x} + \frac{\partial^2 w_0}{\partial x^2} \right) - C_z \Phi + C_x \frac{\partial^2 \Phi}{\partial x^2} - C_{z\Phi} - \rho^2 \left[B_x^{(0)} \frac{\partial^3 u_0}{\partial x^3} + B_x^{(1)} \frac{\partial^3 \varphi_x}{\partial x^3} + B_z^{(0)} \left(\frac{\partial^3 \varphi_x}{\partial x^3} + \frac{\partial^4 w_0}{\partial x^4} \right) - c_1 B_x^{(3)} \left(\frac{\partial^3 \varphi_x}{\partial x^3} + \frac{\partial^4 w_0}{\partial x^4} \right) - c_2 B_z^{(2)} \left(\frac{\partial^3 \varphi_x}{\partial x^3} + \frac{\partial^4 w_0}{\partial x^4} \right) - C_z \frac{\partial^2 \Phi}{\partial x^2} + C_x \frac{\partial^4 \Phi}{\partial x^4} \right] = 0 \quad (21d)$$

where $A_{ij}^{(m)}$, $B_i^{(m)}$, C_i and $C_{i\Phi}$ refer to resultant stiffness, piezoelectric and dielectric coefficients, and are further described in the Appendix.

4.2. Solution procedure and verification

Navier solution technique is employed for a simply supported nanobeam under axial loading in the following manner:

$$\begin{pmatrix} u_0 \\ \varphi_x \\ w_0 \\ \Phi \end{pmatrix} = \sum_{n=1}^{\infty} \begin{pmatrix} \bar{u}_0 \cos(\beta_n x) \\ \bar{\varphi}_x \cos(\beta_n x) \\ \bar{w}_0 \sin(\beta_n x) \\ \bar{\Phi} \sin(\beta_n x) \end{pmatrix} \wedge \beta_n = \frac{n\pi}{L} \quad (22)$$

where \bar{u}_0 , $\bar{\varphi}_x$, \bar{w}_0 , $\bar{\Phi}$ express maximum amplitudes of displacements and electric potential.

The general governing equations are presented in matrix form as

$$[K][\bar{u}_0 \quad \bar{\varphi}_x \quad \bar{w}_0 \quad \bar{\Phi}]^T = 0 \quad (23)$$

where $[K]$ is symmetric 4 x 4 stiffness matrix including in-plane electromechanical forces induced by external loads. Elements of stiffness matrix are presented in [64].

The presented solution scheme, as well as the obtained numerical results, were extensively compared with results from the literature, and verification may be found in [61,64]. Selected numerical results are presented in Tables 1 and 2, showing excellent accordance with results from the literature.

Tab. 1. Dimensionless buckling load $\bar{N}_{cr} = \hat{N}_{xx} \frac{L^2}{EI}$ of simply supported homogeneous nanobeam without piezoelectric layers, assumed properties: $L = 10 \text{ nm}$, $E = 30 \text{ MPa}$, $\nu = 0.3$, $I = \int_{-h/2}^{h/2} z^2 dz$

L/H	g	Beam model assumptions				Present
		Euler-Bernoulli	Timoshenko	Reddy	Thai	
		[45]				
5	0	9.8696	8.9509	8.9519	8.9519	8.9519
	2	8.2426	7.4753	7.4761	7.4761	7.4761
	4	7.0761	6.4174	6.4181	6.4181	6.4181
20	0	9.8696	9.8067	9.8067	9.8067	9.8067
	2	8.2426	8.1900	8.1900	8.1900	8.1901
	4	7.0761	7.0310	7.0310	7.0310	7.0310

Tab. 2. Dimensionless buckling load $\bar{N}_{cr} = \hat{N}_{xx} \frac{12L^2}{E_m h^3}$ of simply supported FG beam without piezoelectric layers, assumed properties: $L = 10 \text{ m}$, $E_c = 380 \text{ GPa}$, $E_m = 70 \text{ GPa}$, $\nu = 0.3$

L/H	g	[68]	[69]	Present
5	0	49.5970	48.5959	48.5959
	1	20.0899	19.6525	19.6525
	5	10.3708	10.1460	10.1460
20	0	53.3175	53.2364	53.2364
	1	20.7541	20.7212	20.7212
	5	10.6341	10.6171	10.6171

5. PARAMETRIC STUDY

The present section contains novel numerical examples of a differences rate that occurs when neither Eringen's nonlocal elasticity nor the strain gradient theory is used in stability analysis of nanostructures. The nonlocal interaction range coefficient is defined as:

$$\delta = \left| \frac{\bar{N}_{cr}^l - \bar{N}_{cr}^{nl}}{\bar{N}_{cr}^l} \right| * 100\% \quad (24)$$

where \bar{N}_{cr}^l and \bar{N}_{cr}^{nl} stand for dimensionless critical buckling load obtained based on the classical (local) theory of elasticity and the nonlocal strain gradient theory. The dimensionless critical load is obtained for both using $\bar{N}_{cr}^i = \hat{N}_{xx}^i \frac{12L^2}{E_c h^3}$, $i = l, nl$, where \hat{N}_{xx}^i is the dimension load value. The studied nanobeam is characterised by unit width and total thickness $H = 10 \text{ nm}$ that consists of FGM porous core thickness $h = 7 \text{ nm}$, and piezoelectric layers thickness $h_p = 1.5 \text{ nm}$. Length of the nanobeam is assumed to be variable while studying the effect of length-to-thickness ratio. Material properties of the nanostructure are taken as the following: $E_c = 380 \text{ GPa}$ and $E_m = 70 \text{ GPa}$ as Young's moduli of FGM core; and $D_{xx} = 226 \text{ GPa}$ and $D_{xz} = 44.2 \text{ GPa}$ as elastic

coefficients of piezoelectric layers. $e_x = -2.2 C/m^2$ and $e_z = 5.8 C/m^2$ are values of piezoelectric permittivity constants, whereas $\epsilon_x = 5.64 \cdot 10^{-9} C/Vm$ and $\epsilon_z = 6.35 \cdot 10^{-9} C/Vm$ are dielectric permittivity constants. Poisson's ratio is assumed to be $\nu = 0.3$ for both piezoelectric face-sheets and FGM core.

First, Fig. 3 presents differences in dimensionless buckling load caused by in-plane mechanical force and external voltage for diverse nonlocal and length scale parameters for diverse length-to-thickness ratios L/H . In this case, we assumed a homogeneous nanobeam ($g = 0$). Nonlocal to length scale parameters ratio is introduced as $\psi = \mathfrak{B} / \ell$ and taken for this study as $\psi = 2 [nm]$ for Fig. 3(a). Then, for Fig. 3(b), the constant value of Eringen's nonlocal coefficient is assumed as $\mathfrak{B} = 0$. Finally, for Fig. 3(c), there is analysis for the pseudorandom ratio of \mathfrak{B} / ℓ . Values for pseudorandom ratio were chosen in manner that enables clearly presenting the impact of size-dependent parameters. It is necessary to analyse diverse relationships between the nonlocal parameter of Eringen and the length scale coefficient because these depend on initial stress, rotary inertia, geometrical aspects ratio and BCs, as well as material properties [70-73]. Table 3 presents selected numerical results, which were further used in Fig. 3(b).

Tab. 3. Differences in dimensionless buckling load for diverse length scale parameter assuming $\mathfrak{B} = 0$

ℓ	0	1.5	3	4.5	6
$L = 50 nm$					
\bar{N}_{cr}^i	6.693	6.753	6.931	7.228	7.645
$\delta(\%)$	0.000	0.888	3.553	7.994	14.212
$L = 100 nm$					
\bar{N}_{cr}^i	7.096	7.112	7.159	7.238	7.349
$\delta(\%)$	0.000	0.222	0.888	1.998	3.553
$L = 150 nm$					
\bar{N}_{cr}^i	7.176	7.184	7.205	7.240	7.290
$\delta(\%)$	0.000	0.099	0.395	0.888	1.579

At this stage, it should be stated that the nonlocal interaction range obtained from mechanical critical buckling load and that from critical voltage (external voltage causing nanobeams' buckling response) are equivalent. This is caused by the fact that electric field contribution is represented in equations of motion as the in-plane electric force acting at the same point as mechanical loads. It should be noted, based on results that have been derived but are not presented here, that for all L/H ratios, material gradations and porosity types along with nanoscale coefficients, the ratio of mechanical buckling load to critical voltage is constant. Therefore, the influence of mechanical loads and applied voltage may be adjusted, based on their relationship to one another, in complexly loaded structures, to omit their buckling response. From Fig. 3, it may be generally observed that, for increasing value of L/H , the impact of size-dependent coefficients decreases. It should be cleared up, that by increasing the length-to-thickness ratio, the nanostructure is lengthened because the constant thickness is assumed. Both the nonlocal coefficient and the length scale parameter have values in nanoscale. Therefore, it may be concluded that nanoscale effects disappear when nanobeam is lengthened to an extent greater than 150 nm. From the

other perspective, the change of thickness of the nanostructure should be examined. Nonetheless, the differential operator in constitutive relations acts in the x -direction, and thus that change does not influence mechanical response. On that account, enhancement of the constitutive relations of the theory may be an important step towards analysing nanoscale effects in diverse directions through nanostructures. The increasing value of the length scale parameter, assuming a constant ratio ψ , generates an initial increase in the δ parameter, then its decrease when ℓ is tending to $\ell = 2 nm$ and finally an increase with further increasing of the length scale parameter. Initial increment of small-scale parameters indicates primary stress and strain gradients from the nonlocal theory.

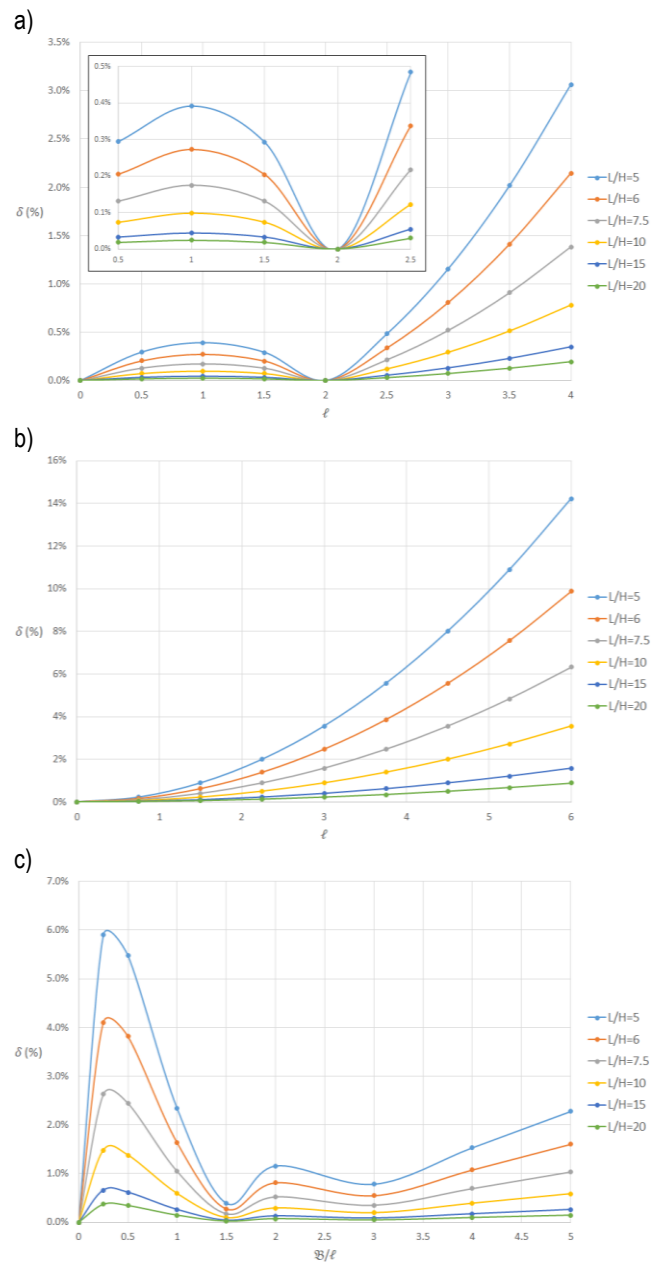


Fig. 3. Effect of length-to-thickness ratio on nonlocal interaction range parameter for dimensionless buckling load as well as critical voltage: (a) constant ratio $\psi = 2 [nm]$; (b) nonlocal parameter $\mathfrak{B} = 0$; (c) pseudorandom ratio of \mathfrak{B}/ℓ

Based on the figure, it may be concluded that this observation gleaned from the present study confirms those of previous studies [74,75] that softening and hardening nonlocal effects disappear when $\ell^2 = \mathfrak{B}$. In that case, size-dependent parameters cancel each other out and both constitutive relations and equations of motion are reduced to classical continuum theory. Another conclusion of this observation is the information that increasing the length scale parameter ℓ generates higher differences between classical and nonlocal buckling responses. The length scale coefficient is coupled with a greater number of derivatives in equations of motion than Eringen's nonlocal parameter. Therefore, increasing the value of ℓ increases the number of additional gradients of strains (hardening effect), and then increase in the differences between classical and nonlocal approaches. Furthermore, as can be seen from Fig. 3(c), appropriate identification of ψ parameter has a key role in obtaining the accurate mechanical response of nanostructures.

Dependence of the nonlocal interaction range parameter for buckling behaviour of homogeneous ($g = 0$) nanobeam on external voltage as well as diverse small-scale parameters is studied in Fig. 4. For this study, it is assumed that $\psi = 1.2 \text{ nm}$ and $L = 100 \text{ nm}$. The positive/negative values of ϕ_0 refer to compression/extension, and in consequence, lead to small shortening/lengthening of the nanostructure. Applying additional electrical loads generate strains and stresses in the structure. Nonlocal gradients of strains and stresses overlap with electrically generated ones, and consequently, their influence on the buckling behaviour is increased. Increasing positive values of critical voltage cause an increase in the nonlocal interaction range, and, contrariwise, a negative value of external voltage decreases the interaction range parameter values, because positive and negative voltage values induce compression and tension of the structure. It should be also observed that compressively acting external voltage has a higher impact on the difference in the obtained results. This can be explained based on the position that compressive force generates higher induced stresses, a beam is shortened and bent, and consequently the nonlocal interaction is stronger in comparison to an unloaded structure.

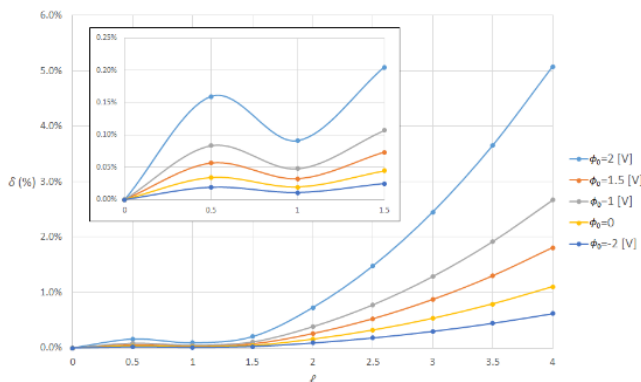


Fig. 4. Effect of external electric voltage and size-dependent parameters on nonlocal interaction range parameter for dimensionless buckling response of the nanobeam

The impact of a material gradation through the nanobeams' core thickness in conjunction with pseudorandom distribution of small-scale coefficient on the nonlocal interaction range parameter for buckling response is studied for diverse aspect ratios and displayed in Fig. 5. Selected results, for nanobeam with

$L = 150 \text{ nm}$, are presented in Tab. 4. In the current investigation, the nanobeam is subjected to in-plane electric forces induced by external voltage $\phi_0 = 0.65 \text{ V}$. The difference between the results obtained from classical and nonlocal based approaches is notably higher for a higher ratio of L / H . It is worth noting that for homogeneous ($g = 0$) structure, the nonlocal interaction range parameter is lower for a higher length-to-thickness ratio, which is consistent with results presented previously. The influence of size-dependent coefficients is similar to that observed in previous cases. Nevertheless, for nanostructure with a higher L / H ratio, the difference increases remarkably with increasing the power-law index g . The higher the power-law index value, the softer the structure becomes, and thus the lower is the force needed to buckle the structure. Considering applied electrical force, increasing g index causes that structure to be near to the buckling. From this, we infer that the effect of small-scale parameters is considerably greater when the structure is under loads that are near to critical value. Even if we use nonlocal differential operator for abscissa, gradation of the material parameters through beam thickness has an indirect impact on the behaviour of structure (stress concentration, bending). Thus, shortening and extension are significantly dependent on this material distribution as well as a direct effect of nonlocal parameters.

Tab. 4. Differences in dimensionless buckling load for diverse nonlocal coefficients and the power law index for nanobeam with $L = 150 \text{ nm}$

\mathfrak{B} / ℓ	$\delta(\%)$					
	g					
	0	1	2	3	4	5
0	0.000	0.000	0.000	0.000	0.000	0.000
0.25	1.516	3.179	4.805	5.978	6.746	7.250
0.5	1.415	2.965	4.483	5.577	6.294	6.763
1	0.606	1.271	1.920	2.389	2.696	2.897
1.5	0.101	0.211	0.320	0.398	0.449	0.483
2	0.302	0.634	0.959	1.193	1.346	1.447
3	0.202	0.424	0.640	0.796	0.899	0.966
5	0.604	1.267	1.915	2.382	2.688	2.888

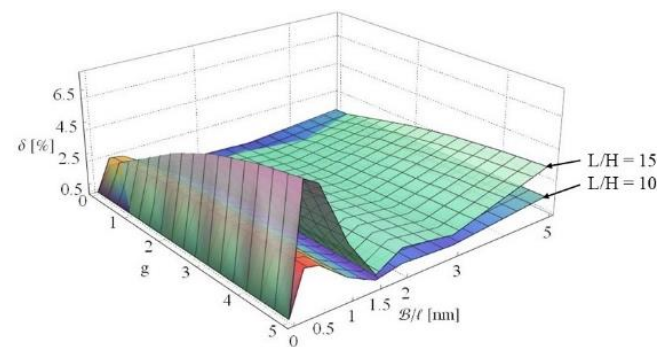


Fig. 5. Effect of material gradation, size-dependent parameters and length-to-thickness ratio on nonlocal interaction range parameter for dimensionless buckling response of the nanobeam

Figure 6 shows an effect of diverse porosity distributions together with a volume of voids on nonlocal interaction range parameter for buckling behaviour of nanobeam ($g = 0$) with a different length-to-thickness ratio that is subjected to external

electric voltage $\phi_0 = 1.5 V$. For this study, size-dependent parameters are fixed as $\ell = 4 nm$ and $\mathcal{B} = 1 nm^2$. Analogous to the previous study, as a result of increasing the length of the nanobeam, the value of the nonlocal interaction range parameter decreases. Further, as a result of enlargement in nanobeam length, nano-scaled size-dependent coefficients have less influence on the mechanical response of the nanostructure. On the other hand, increasing volume of voids (ϑ) magnifies differences between classical and nonlocal buckling responses, regardless of porosity distribution. Differences in obtained results for diverse porosity accumulation follow from different impacts on material resultant stiffness. With the higher L/H ratio and porosity parameter ϑ , the applied voltage is closer to the critical value. It is clearly observed that as the buckling point approaches, the impact of nano-scale coefficients increases.

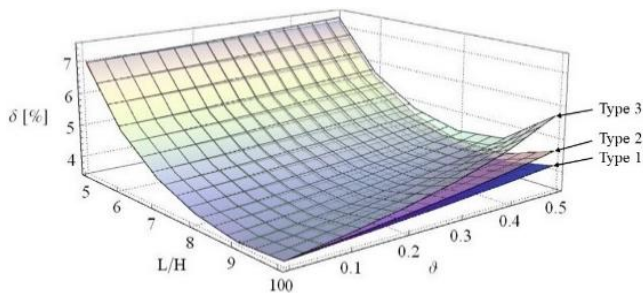


Fig. 6. Effect of length-to-thickness ratio and porosity distribution on nonlocal interaction range parameter for dimensionless buckling response of the nanobeam

Next, the difference between classical and nonlocal based critical porosity is provided. Critical porosity is defined as the volume of voids in the structure, under constant compressive forces, that leads to its buckling. The nonlocal interaction range parameter is obtained in a way that is parallel to the procedure used to derive the buckling-load-based parameters. The impact of diverse porosity distribution in conjunction with nonlocal parameters is displayed in Tab. 5 and Fig. 7. In this case it is considered homogeneous ($g = 0$), but porous nanostructure under in-plane compressive forces $\hat{N}_{xx} = 35 N$. Nonlocal to length scale parameters ratio is assumed $\psi = 2 [nm]$, and length of the structure as $L = 75 nm$. Analogous to critical loads, increasing size-dependent parameters increases differences between critical porosity obtained based on classical and nonlocal theories because it strengthens the influence on higher derivatives in equations of motion. Further, increasing nano-scale coefficients' values leads to widening of the differences between Type 1 porosity and Types 2 and 3. The effects of Type 2 and Type 3 porosity distribution are very similar because both are characterised by zero volume of voids in the mid-plane where compressive force is acting; and consequently, they have a similar impact on nanostructure characteristics.

Continuing the previous investigation, the effect of the diverse ratios of nonlocal to length scale coefficients together with the power-law index (g) on nonlocal interaction range parameter for critical porosity is presented in Fig. 8. In this study, it is assumed $L = 100 nm$ and in-plane mechanical force $\hat{N}_{xx} = 13 N$. Likewise, in the previous study, the values of the nonlocal interaction range parameter for Types 2 and 3 are close, and for Type 1 the value is significantly lower, regardless of the power-law index. Further, the impact of nonlocal parameters increases resultant to

increasing the power-law index. The higher the value of the index, the lower the resultant stiffness, and consequently, the applied compressive force is closer to the critical one. The study also supplements the statement that appropriate identification of Eringen's nonlocal to length scale parameter ratio is crucial in properly anticipating the mechanical response of nanostructures regardless of their homogeneity or inhomogeneity.

Tab. 5. Differences in critical porosity for diverse nonlocal coefficients ratio for nanobeam with $L = 75 nm$

	ℓ				
	0	1	2	3	4
TYPE 1					
ϑ_{cr}^i	0.563	0.555	0.563	0.584	0.620
$\delta(\%)$	0.000	1.317	0.000	3.871	10.120
TYPE 2					
ϑ_{cr}^i	0.396	0.390	0.396	0.412	0.439
$\delta(\%)$	0.000	1.400	0.000	4.139	10.894
TYPE 3					
ϑ_{cr}^i	0.266	0.262	0.266	0.277	0.295
$\delta(\%)$	0.000	1.414	0.000	4.182	11.020

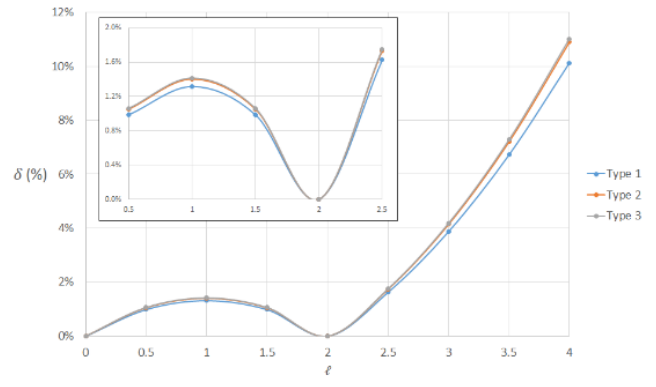


Fig. 7. Effect of porosity distribution and size-dependent parameters on nonlocal interaction range parameter for critical porosity of the nanobeam

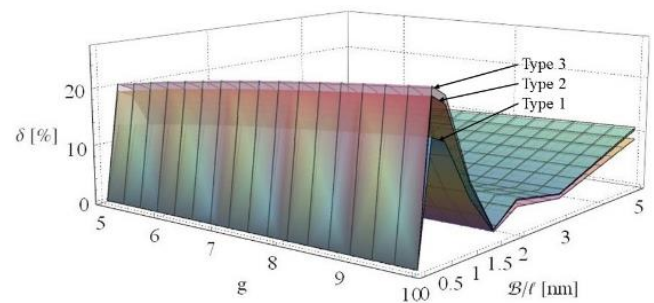


Fig. 8. Effect of porosity distribution and size-dependent parameters on nonlocal interaction range parameter for critical porosity of the nanobeam

6. CONCLUSIONS

The current investigation presents an analysis of differences in the mechanical stability of nanostructures obtained based on

classical and nonlocal theories. The smart nanostructure is considered as FG porous nanobeam with piezoelectric layers. FGM parameters are achieved by using modified Voigt's rule of mixtures and assessing the contribution of an electric field based on a combination of half-cosine and linear variations of the electric potential. Employed equations of motion include both Eringen's nonlocal coefficient and length scale parameter based on the nonlocal strain gradient theory. In the modelling of the operation environment in NEMS devices, the nanostructure is subjected to mechanical in-plane forces and electric field. The utilised refined Reddy third-order shear deformation theory allows adopting the beam model to a wide range of structures without committing errors arising from other beam models' assumptions. The presented results include effects of diverse Eringen's to length scale parameters, nanobeams length-to-thickness ratio, material gradation and porosity distributions, as well as external loadings on the stability of nano-scaled smart beam, supplemented with interpretation and discussion.

In the study, we defined the nonlocal interaction range parameter and checked the boundaries between an application of classical and nonlocal elasticity theories for intelligent nanobeam. The investigation presents a comprehensive model of nano-scaled structure that complies with a previously presented study claiming that size-dependent parameters depend on initial stress and geometrical aspects, as well as material properties. The consideration demonstrates that the influence of size-dependent coefficients decreases resultant to increase in geometrical parameters of the structure. On the other hand, the analysis shows that applied force (especially near to the critical value), as well as material properties, have a significant influence on the importance of nonlocal parameters in the modelling of nanostructures. The conducted study furthers the knowledge and understanding of nonlocal parameters' effects on the stability of smart nanostructures that are an important component of NEMS. Consequently, the results of the study positively impact the possibility of optimisation and control of NEMS devices. Nonetheless, simplified constitutive equations [see Eq. (5)] may not be sufficient in specific conditions; therefore, future studies should focus on influence of the non-equal nonlocal coefficients e_1 and e_0 . Further, improving constitutive relations, including multidimensional differential operator, may be an important improvement of the theory, especially for nonhomogeneous nanostructures.

REFERENCES

- Bhushan B. (Ed.) Springer Handbook of Nanotechnology. Springer-Verlag; 2004.
- Zhao Q, Gan Z, Zhuang Q. Electrochemical sensors based on carbon nanotubes. *Electroanalysis: An International Journal Devoted to Fundamental and Practical Aspects of Electroanalysis*. 2002;14: 1609–1613.
- Briscoe J, Dunn S. Piezoelectric nanogenerators – a review of nanostructured piezoelectric energy harvesters. *Nano Energy*. 2015;14: 15–29.
- Fennimore A, Yuzvinsky T, Han W-Q, Fuhrer M, Cumings J, Zettl A. Rotational actuators based on carbon nanotubes. *Nature*. 2003;424: 408-410.
- Ghayesh MH, Farajpour A. A review on the mechanics of functionally graded nanoscale and microscale structures. *International Journal of Engineering Science*. 2019;137: 8-36.
- Lu L, Guo X, Zhao J. A unified nonlocal strain gradient model for nanobeams and the importance of higher order terms. *International Journal of Engineering Science*. 2017;119, 265-277.
- Toupin RA. Elastic materials with couple-stresses. *Archive for Rational Mechanics and Analysis*. 1962;11: 385-414.
- Mindlin RD, Tiersten HF. Effects of couple-stresses in linear elasticity. *Archive for Rational Mechanics and Analysis*. 1962;11: 415-448.
- Koiter WT. Couple stresses in the theory of elasticity. I and II. *Nederl Akad Wetensch Proc Ser B*. 1964;67: 17-44.
- Yang F, Chong ACM, Lam DCC, Tong P. Couple stress based strain gradient theory for elasticity. *International Journal of Solids and Structures*. 2002;39: 2731-2743.
- Mindlin RD. Micro-structure in linear elasticity. *Archive for Rational Mechanics and Analysis*. 1964;16: 51-78.
- Mindlin RD. Second gradient of strain and surface-tension in linear elasticity. *International Journal of Solids and Structures*. 1965;1: 417-438.
- Lam DCC, Yang F, Chong ACM, Wang J, Tong P. Experiments and theory in strain gradient elasticity. *Journal of the Mechanics and Physics of Solids*. 2003;51: 1477-1508.
- Kroner E. Elasticity theory of materials with long range cohesive forces. *International Journal of Solids and Structures*. 1967;3: 731-742.
- Eringen AC. Nonlocal polar elastic continua. *International Journal of Engineering Science*. 1972;10: 1-16.
- Eringen AC. Linear theory of nonlocal elasticity and dispersion of plane waves. *International Journal of Engineering Science*. 1972;10: 425-435.
- Eringen AC, Edelen DGB. On nonlocal elasticity. *International Journal of Engineering Science*. 1972;10: 233-248.
- Eringen AC. On differential equations of nonlocal elasticity and solutions of screw dislocation and surface wave. *Journal of Applied Physics*. 1983;54: 4703-4710.
- Romano G, Barretta R. Nonlocal elasticity in nanobeams: the stress-driven integral model. *International Journal of Engineering Science*. 2017;115: 14-27.
- Yang B, Vehoff H. Dependence of nanohardness upon indentation size and grain size – A local examination of the interaction between dislocations and grain boundaries. *Acta Materialia*. 2007;55: 849-856.
- Voyiadjis GZ, Peters R. Size effects in nanoindentation: an experimental and analytical study. *Acta Mechanica*. 2010;211: 131-153.
- Askes H, Aifantis EC. Gradient elasticity and flexural wave dispersion in carbon nanotubes. *Physical Review B*. 2009;80: 195412.
- Lim CW, Zhang G, Reddy JN. A higher-order nonlocal elasticity and strain gradient theory and its applications in wave propagation. *Journal of the Mechanics and Physics of Solids*. 2015;78, 298-313.
- Demir Ç, Civalek Ö. Torsional and longitudinal frequency and wave response of microtubules based on the nonlocal continuum and nonlocal discrete models. *Applied Mathematical Modelling*. 2013;37: 9355-9367.
- Akgöz B, Civalek Ö. Longitudinal vibration analysis for microbars based on strain gradient elasticity theory. *Journal of Vibration and Control*. 2014;20: 606-616.
- Cornacchia F, Fabbrocino F, Fantuzzi N, Luciano R, Pena R. Analytical solution of cross- and angle-ply nano plates with strain gradient theory for linear vibrations and buckling. *Mechanics of Advanced Materials and Structures*. 2021;28: 1201-1215.
- Žur KK, Farajpour A, Lim CW, Jankowski P. On the nonlinear dynamics of porous composite nanobeams connected with fullerenes. *Composite Structures*. 2021;274: 114356.
- Monaco GT, Fantuzzi N, Fabbrocino F, Luciano R. Critical Temperatures for Vibrations and Buckling of Magneto-Electro-Elastic Nonlocal Strain Gradient Plates. *Nanomaterials*. 2021;11: 87.
- Jalaei MH, Ghorbanpour Arani A, Nguyen-Xuan H. Investigation of thermal and magnetic field effects on the dynamic instability of FG Timoshenko nanobeam employing nonlocal strain gradient theory. *International Journal of Mechanical Sciences*. 2019;161-162: 105043.

30. Żur KK, Arefi M, Kim J, Reddy JN. Free vibration and buckling analyses of magneto-electro-elastic FGM nanoplates based on nonlocal modified higher-order sinusoidal shear deformation theory. *Composites Part B: Engineering*. 2020;182: 107601.
31. Zhao X, Zheng S, Li Z. Effects of porosity and flexoelectricity on static bending and free vibration of AFG piezoelectric nanobeams. *Thin-Walled Structures*. 2020;151: 106754.
32. Faghidian SA, Żur KK, Pan E, Kim J. On the analytical and meshless numerical approaches to mixture stress gradient functionally graded nano-bar in tension. *Engineering Analysis with Boundary Elements*. 2022;134: 571-580.
33. Barretta R, Caporale A, Faghidian SA, Luciano R, Marotti de Sciarra F, Medaglia CM. A stress-driven local-nonlocal mixture model for Timoshenko nano-beams. *Composites Part B: Engineering*. 2019;164: 590-598.
34. Barretta R, Fazelzadeh SA, Feo L, Ghavanloo E, Luciano R. Nonlocal inflected nano-beams: A stress-driven approach of bi-Helmholtz type. *Composite Structures*. 2018;200: 239-245.
35. Barretta R, Faghidian SA, Luciano R, Medaglia CM, Penna R. Stress-driven two-phase integral elasticity for torsion of nano-beams. *Composites Part B: Engineering*. 2018;145: 62-69.
36. Jalaei MH, Thai HT, Civalek Ö. On viscoelastic transient response of magnetically imperfect functionally graded nanobeams. *International Journal of Engineering Science*. 2022;172: 103629.
37. Monaco GT, Fantuzzi N, Fabbrocino F, Luciano R. Trigonometric Solution for the Bending Analysis of Magneto-Electro-Elastic Strain Gradient Nonlocal Nanoplates in Hygro-Thermal Environment. *Mathematics*. 2021;9: 567.
38. Penna R, Feo L, Lovisi G., Hygro-thermal bending behavior of porous FG nano-beams via local/nonlocal strain and stress gradient theories of elasticity. *Composite Structures*. 2021;263: 113627.
39. Monaco GT, Fantuzzi N, Fabbrocino F, Luciano R. Semi-analytical static analysis of nonlocal strain gradient laminated composite nanoplates in hygrothermal environment. *Journal of the Brazilian Society of Mechanical Sciences and Engineering*. 2021;43: 274.
40. Faghidian SA, Żur KK, Reddy JN. A mixed variational framework for higher-order unified gradient elasticity. *International Journal of Engineering Science*. 2022;170: 103603.
41. Apuzzo A, Barretta R, Faghidian SA, Luciano R, Marotti de Sciarra F. Nonlocal strain gradient exact solutions for functionally graded inflected nano-beams. *Composites Part B: Engineering*. 2019;164: 667-674.
42. Reddy JN. Nonlocal theories for bending, buckling and vibration of beams. *International Journal of Engineering Science*. 2007;45: 288-307.
43. Aydogdu M. A general nonlocal beam theory: Its application to nano-beam bending, buckling and vibration. *Physica E: Low-dimensional Systems and Nanostructures*. 2009;41: 1651-1655.
44. Roque CMC, Ferreira AJM, Reddy JN. Analysis of Timoshenko nanobeams with a nonlocal formulation and meshless method. *International Journal of Engineering Science*. 2011;49: 976-984.
45. Thai HT. A nonlocal beam theory for bending, buckling, and vibration of nanobeams. *International Journal of Engineering Science*. 2012;52: 56-64.
46. Thai HT, Vo TP. A nonlocal sinusoidal shear deformation beam theory with application to bending, buckling, and vibration of nanobeams. *International Journal of Engineering Science*. 2012;54: 58-66.
47. Ghannadpour SAM, Mohammadi B, Fazilati J. Bending, buckling and vibration problems of nonlocal Euler beams using Ritz method. *Composite Structures*. 2013;96: 584-589.
48. Şimşek M, Yurtcu HH. Analytical solutions for bending and buckling of functionally graded nanobeams based on the nonlocal Timoshenko beam theory. *Composite Structures*. 2013;97: 378-386.
49. Rahmani O, Jandaghian AA. Buckling analysis of functionally graded nanobeams based on a nonlocal third-order shear deformation theory. *Applied Physics A*. 2015;119: 1019-1032.
50. Chaht FL, Kaci A, Houari MSA, Tounsi A, Bég OA, Mahmoud SR. Bending and buckling analyses of functionally graded material (FGM) size-dependent nanoscale beams including the thickness stretching effect. *Steel and Composite Structures*. 2015;18: 425-442.
51. Yu YJ, Xue Z-N, Li C-L, Tian X-G. Buckling of nanobeams under nonuniform temperature based on nonlocal thermoelasticity. *Composite Structures*. 2016;146: 108-113.
52. Nejad MZ, Hadi A, Rastgoo A. Buckling analysis of arbitrary two-directional functionally graded Euler-Bernoulli nano-beams based on nonlocal elasticity theory. *International Journal of Engineering Science*. 2016;103: 1-10.
53. Li X, Li L, Hu Y, Ding Z, Deng W. Bending, buckling and vibration of axially functionally graded beams based on nonlocal strain gradient theory. *Composite Structures*. 2017;165: 250-265.
54. Tuna M, Kirca M. Bending, buckling and free vibration analysis of Euler-Bernoulli nanobeams using Eringen's nonlocal integral model via finite element method. *Composite Structures*. 2017;179: 269-284.
55. Mirjavadi SS, Afshari MB, Khezek M, Shafiei N, Rabby S, Kordnejad M. Nonlinear vibration and buckling of functionally graded porous nanoscaled beams. *Journal of Brazilian Society of Mechanical Sciences and Engineering*. 2018;40: 352.
56. Khaniki HB, Hosseini-Hashemi Sh, Nezamabadi A. Buckling analysis of nonuniform nonlocal strain gradient beams using generalized differential quadrature method. *Alexandria Engineering Journal*. 2018;57: 1361-1368.
57. Alibeigi B, Tadi Beni Y. On the size-dependent magneto/electromechanical buckling of nanobeams. *European Physical Journal Plus*. 2018;133: 398.
58. Alibeigi B, Tadi Beni Y, Mehralian F. On the thermal buckling of magneto-electroelastic piezoelectric nanobeams. *European Physical Journal Plus*. 2018;133: 133.
59. Xiao W, Gao Y, Zhu H. Buckling and post-buckling of magneto-electro-thermo-elastic functionally graded porous nanobeams. *Microsystem Technologies*. 2019;25: 2451-2470.
60. Hashemian M, Foroutan S, Toghraie D. Comprehensive beam models for buckling and bending behavior of simple nanobeam based on nonlocal strain gradient theory and surface effects. *Mechanics of Materials*. 2019;139: 103209.
61. Jankowski P, Żur KK, Kim J, Reddy JN. On the bifurcation buckling and vibration of porous nanobeams. *Composite Structures*. 2020;250: 112632.
62. Civalek Ö, Uzun B, Yayli MÖ. Stability analysis of nanobeams placed in electromagnetic field using a finite element method. *Arabian Journal of Geoscience*. 2020;13: 1165.
63. Civalek Ö, Uzun B, Yayli MÖ. Finite element formulation for nano-scaled beam elements, ZAMM – Journal of Applied Mathematics and Mechanics. 2021:e202000377.
64. Jankowski P, Żur KK, Kim J, Lim CW, Reddy JN. On the piezoelectric effect on stability of symmetric FGM porous nanobeams. *Composite Structures*. 2021;267: 113880.
65. Eringen AC. *Nonlocal Continuum Field Theories*, Springer;2002.
66. Reddy JN. *Energy principles and variational methods in applied mechanics*. John Wiley & Sons;2017.
67. Wang Q. On buckling of column structures with a pair of piezoelectric layers. *Engineering Structures*. 2002;24(2): 199-205.
68. Nguyen T-K, Vo TP, Nguyen B-D, Lee J. An analytical solution for buckling and vibration analysis of functionally graded sandwich beams using a quasi-3D shear deformation theory. *Composite Structures*. 2016;156: 238-252.
69. Vo TP, Thai HT, Nguyen T-K, Maheri A, Lee J. Finite element model for vibration and buckling of functionally graded sandwich beams based on a refined shear deformation theory. *Engineering Structures*. 2014;64: 12-22.
70. Ghavanloo E, Fazelzadeh SA. Evaluation of nonlocal parameter for single-walled carbon nanotubes with arbitrary chirality. *Meccanica*. 2016;51: 41-54.

71. Thai HT, Vo TP, Nguyen TK, Kim SE. A review of continuum mechanics models for size-dependent analysis of beams and plates. *Composite Structures*. 2017;177: 196-219.
72. Zhang Z, Wang CM, Challamel N. Eringen's length scale coefficient for buckling of nonlocal rectangular plates from microstructured beam-grid model. *International Journal of Solids and Structures*. 2014;51: 4307-4315.
73. Mehralian F, Tadi Beni Y, Zeverdejani MK. Calibration of nonlocal strain gradient shell model for buckling analysis of nanotubes using molecular dynamics simulations. *Physica B: Condensed Matter*. 2017;521: 102-111.
74. Zeighampour H, Tadi Beni Y. Size dependent analysis of wave propagation in functionally graded composite cylindrical microshell reinforced by carbon nanotube. *Composite Structures*. 2017;179: 124-131.
75. Lu L, Guo X, Zhao J. Size-dependent vibration analysis of nano-beams based on the nonlocal strain gradient theory. *International Journal of Engineering Science*. 2017;116: 12–24.

The work has been conducted within WZ/WM-IIM/3/2020 project and was financed by the funds of the Ministry of Science and Higher Education, Poland

Piotr Jankowski:  <https://orcid.org/0000-0003-4137-5899>

Appendix

$$\{A_{xx}^{(0)}, A_{xx}^{(1)}, A_{xx}^{(2)}, A_{xx}^{(3)}, A_{xx}^{(4)}, A_{xx}^{(6)}\} = b \int_{-h/2-h_p}^{h/2} D_{xx}\{1, z, z^2, z^3, z^4, z^6\} dz + b \int_{-h/2}^0 C_{xx}\{1, z, z^2, z^3, z^4, z^6\} dz + b \int_0^{h/2} C_{xx}\{1, z, z^2, z^3, z^4, z^6\} dz + b \int_{h/2}^{h/2+h_p} D_{xx}\{1, z, z^2, z^3, z^4, z^6\} dz, \tag{A.1}$$

$$\{A_{xz}^{(0)}, A_{xz}^{(2)}, A_{xz}^{(4)}\} = b \int_{-h/2-h_p}^{h/2} D_{xz}\{1, z^2, z^4\} dz + b \int_{-h/2}^0 C_{xz}\{1, z^2, z^4\} dz + b \int_0^{h/2} C_{55}\{1, z^2, z^4\} dz + b \int_{h/2}^{h/2+h_p} D_{xz}\{1, z^2, z^4\} dz, \tag{A.2}$$

$$\{B_x^{(0)}, B_x^{(1)}, B_x^{(3)}\} = b \int_{-h/2-h_p}^{h/2} e_x \frac{\pi}{h_p} \sin\left(\frac{\pi z_2}{h_p}\right) \{1, z, z^3\} dz + b \int_{h/2}^{h/2+h_p} e_x \frac{\pi}{h_p} \sin\left(\frac{\pi z_1}{h_p}\right) \{1, z, z^3\} dz, \tag{A.3}$$

$$\{B_z^{(0)}, B_z^{(2)}\} = b \int_{-h/2-h_p}^{h/2} e_z \cos\left(\frac{\pi z_2}{h_p}\right) \{1, z^2\} dz + b \int_{h/2}^{h/2+h_p} e_z \cos\left(\frac{\pi z_1}{h_p}\right) \{1, z^2\} dz, \tag{A.4}$$

$$\{B_{x\phi}^{(0)}, B_{x\phi}^{(1)}, B_{x\phi}^{(3)}\} = b \int_{-h/2-h_p}^{h/2} e_x \frac{2}{h_p} \phi_0 \{1, z, z^3\} dz + b \int_{h/2}^{h/2+h_p} e_x \frac{2}{h_p} \phi_0 \{1, z, z^3\} dz, \tag{A.5}$$

$$C_x = b \int_{-h/2-h_p}^{h/2} \epsilon_x \left(\cos\left(\frac{\pi z_2}{h_p}\right)\right)^2 dz + b \int_{h/2}^{h/2+h_p} \epsilon_x \left(\cos\left(\frac{\pi z_1}{h_p}\right)\right)^2 dz, \tag{A.6}$$

$$C_z = b \int_{-h/2-h_p}^{h/2} \epsilon_z \left(\frac{\pi}{h_p} \sin\left(\frac{\pi z_2}{h_p}\right)\right)^2 dz + b \int_{h/2}^{h/2+h_p} \epsilon_z \left(\frac{\pi}{h_p} \sin\left(\frac{\pi z_1}{h_p}\right)\right)^2 dz, \tag{A.7}$$

$$C_{z\phi} = b \int_{-h/2-h_p}^{h/2} \epsilon_z \frac{2}{h_p} \phi_0 \frac{\pi}{h_p} \sin\left(\frac{\pi z_2}{h_p}\right) dz + b \int_{h/2}^{h/2+h_p} \epsilon_z \frac{2}{h_p} \phi_0 \frac{\pi}{h_p} \sin\left(\frac{\pi z_1}{h_p}\right) dz. \tag{A.8}$$